3-2010

Three-dimensional Acceleration Measurement Using Videogrammetry Tracking Data

Jack Leifer
Trinity University, jleifer@trinity.edu

Bryan J. Weems
Trinity University

Sean C. Kienle
Trinity University

Aaron M. Sims
Trinity University

Three-dimensional Acceleration Measurement Using Videogrammetry Tracking Data

Jack Leifer
Associate Professor

Bryan Weems, Sean C. Kienle and Aaron M. Sims
Undergraduate Research Assistants
Trinity University Department of Engineering Science
One Trinity Place
San Antonio, TX 78212
(210) 999-7564
(210) 999-8037 (FAX)

ABSTRACT

In order to evaluate the feasibility of multi-point, non-contact, acceleration measurement, a high-speed, precision videogrammetry system has been assembled from commercially-available components and software. Consisting of three synchronized 640 X 480 pixel monochrome progressive scan CCD cameras each operated at 200 frames per second, this system has the capability to provide surface-wide position-versus-time data that are filtered and twice-differentiated to yield the desired acceleration tracking at multiple points on a moving body. The oscillating motion of targets mounted on the shaft of a modal shaker were tracked, and the accelerations calculated using the videogrammetry data were compared directly to conventional accelerometer measurements taken concurrently. Although differentiation is an inherently noisy operation, the results indicate that simple mathematical filters based on the well-known Savitzky and Golay algorithms, implemented using spreadsheet software, remove a significant component of the noise, resulting in videogrammetry-based acceleration measurements that are comparable to those obtained using the accelerometers.

I. Introduction

The options for measuring in- and out-of-plane acceleration profile across the extent of a moving or deforming body or structure are relatively limited. (1) Lightweight, multi-axis accelerometers, though becoming ubiquitous, generally require cables that extend between the test object and the data-acquisition system. There are some applications, including the measurement of human motion, where physical cables can affect, or even hinder, the motion being measured. In addition, the dynamics of certain systems, such as the thin-film shells described by

Denoyer et al [1], will be affected by the mass of any accelerometer used to monitor its motion, especially if multiple accelerometers are required in order to obtain measurements at more than one location simultaneously. Finally, the low-frequency response of most lightweight accelerometers is quite poor, which means that they are not well-suited for the measurement of either rigid-body motion or structures that respond at extremely low frequencies. (2) Certain noncontact approaches, including LASER vibrometers [2] and capacitive sensors [3], are only capable of measuring out-of-plane position data at one discrete point. While full-field, out-of-plane data can be obtained by performing successive measurements while scanning across the surface of the test article, such an approach is prohibitively slow when surface-wide dynamic information is required. Furthermore, these approaches cannot be used to obtain in-plane motion components. (3) Other approaches that can be used for measuring in-plane surface displacement, including electronic laser speckle interferometry (ELSI) and moiré interferometry, are also inherently capable of true simultaneous full-field displacement measurement, which could potentially be post-processed to obtain the corresponding in-plane acceleration components. However, neither approach has sufficient dynamic range to measure large-scale motion [4].

Another potential measurement approach, described herein, obtains the necessary tracking data via a non-contact technique that uses video images of a moving test article taken by multiple, synchronized video cameras. Using appropriate data processing techniques, this approach can efficiently generate the full-field, in- and out-of-plane acceleration profile of a moving, deforming object. Dating from the 1970s, *videogrammetry* has been used to track the position of rigid as well as deforming flexible bodies as they move, especially in the medical, automotive, and astronautical fields [5-9]. The technique is a direct extension of photogrammetry, a well-established method for performing three-dimensional shape reconstructions of an object using a set of simultaneously triggered images [10]. The major difference between photogrammetry and videogrammetry is that the latter performs successive three-dimensional shape reconstructions, and hence enables full-field (multi-point) position tracking through the duration of the image sequence. Regardless of whether a static (single-image set) or dynamic (multiple sequence of image sets) reconstruction is sought, the method determines the three-dimensional shape based on a single set of images taken simultaneously from a number of vantage points, by calculating the location of discrete points distributed on the surface of the test object, via triangulation Most often, such points consist of high-contrast circular targets that are placed on the test object prior to imaging; the exact location of each point corresponds to the target centroid. Targets can be directly drawn on the surface of a test

article (e.g. using a “sharpie” marker); flexible, adhesive-backed materials can be “stuck” to the surface to serve as markers; or other methods of generating targets, such as direct surface etching, can be employed [9].

This paper explores the viability of using the videogrammetric-based reconstructions to track, via straightforward post-processing of measured position data, the in- and out-of-plane acceleration components of one or more individual points on the surface of the test article (here, a shaft driven by a modal shaker to demonstrate proof of concept). In order to verify the calculated accelerations extracted using the measured videogrammetric displacement data, an accelerometer was mounted on the shaker shaft, which was excited at various combinations of amplitude, frequency, and axis orientation. Visible targets were mounted immediately below the accelerometer; the in- and out-of-plane acceleration components of the targets’ motion obtained using the videogrammetry-based approach were directly compared to the output of the calibrated accelerometer. As videogrammetry-based measurements naturally yield position, and not acceleration data, post-processing approaches such as numerical differentiation and filtering were used to obtain the desired acceleration data.

II. Camera Placement, System Calibration and Lighting

The videogrammetry system utilized in this research (an improved version of the one described in Leifer et al. [9]) consisted of three synchronized 640 X 480 pixel monochrome progressive scan CCD cameras (JAI Pulnix model TM-6740G), each capable of capturing images at 200 frames per second, which were equipped with 9-mm narrow-angle lenses. The three cameras were intended to capture images simultaneously from three distinct viewpoints; each one recorded video to a dedicated 36.7 GB SCSI hard drive. Streams5 software (IO Industries, London, Ontario, Canada) was used to view, edit and export the video data. Image synchronization was verified (to within one frame) through the use of an LED digital event timer, capable of displaying time to 0.01 seconds. The counter was placed so that its display remained within the view of each tracking camera. Each set of simultaneous images acquired by the cameras allowed the targets to be located in three-dimensional space using the principles of triangulation.

For the measurements reported herein, the video cameras were placed at three different heights in a “fan” shape, as shown in Figure 1. Two cameras were placed approximately the same distance from the subject, while a third camera was placed closer to the subject, bisecting the angle between the outer two. The approximate angle between each camera axis was set to 45^{o}. Increasing the angle between each camera to 60^{o} – 90^{o} may have

increased measurement accuracy by a small amount; physical constraints prevented us from doing so for this experimental. After all the cameras were positioned, the focal lengths of the outer two cameras were increased, in order to decrease their respective field of view to that of the third. Once the settings of all three cameras were finalized, each was individually calibrated using the semi-automated procedure provided by PhotoModeler6 (Eos Systems, Vancouver, Canada), the videogrammetry software used for this work [11]. Calibration removed the effects of the internal characteristics of each camera (e.g. focal length, lens distortion) from the three-dimensional reconstruction.

In addition to camera placement, another important factor in obtaining accurate videogrammetric tracking data involves defining a standard fixed coordinate system for purposes of image calibration. In order to properly scale the image from each camera, it was essential that at least two of the three major axes (X, Y, and Z) be identified and visible in all three cameras' field of vision without obscuring the view of the test article. As this set of experiments involved the tracking of harmonic motions over a small (10-15 mm) range, a two-axis coordinate system consisting of 11-mm diameter black dots on 29-mm centers was laser-printed on to standard white office paper. The dot diameter was selected to allow a standard 8-10 pixel diameter when viewed by the Pulnix cameras (Figure 2). Scaling of the workspace within PhotoModeler requires affixing the coordinate grid to a flat surface, and then defining (within the software) the direction of absolute x-direction (horizontal); absolute y-direction (vertical), and a known fixed distance defined by two of the targets.

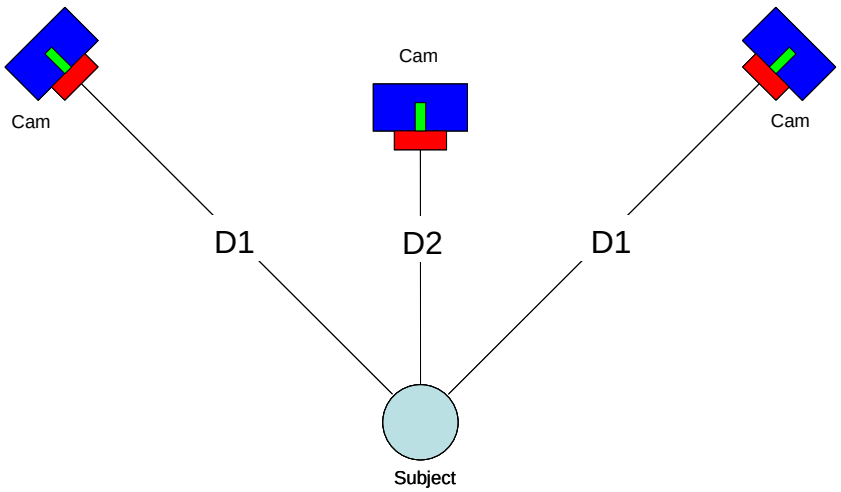

Fig. 1: Videogrammetric camera placement, shown from above. Though not apparent from this schematic, each camera was placed at a unique height.

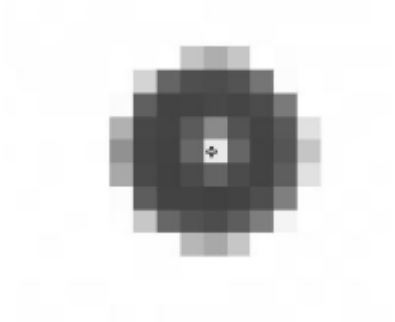

Fig. 2: Zoomed view of a circular, 11-mm black-on-white coordinate-system target, as viewed by one of the videogrammetric cameras. The target diameter corresponds to approximately 9 pixels on the camera's imaging element, equal to a ratio of about 1.22 mm per imaging element pixel. The small "plus" near the center of the image indicates the exact tracking location, which corresponds to the target centroid.

This information serves as the basis of the triangulation algorithm used by PhotoModeler to locate the cameras, as well as the location of any other tracked targets within the imaged workspace.

Clearly, the precision and accuracy to which the imaged workspace is calibrated helps determines the precision and accuracy of tracking. In order to improve tracking performance, the location of each target on the wall-mounted coordinate system grid was verified using a Leica Total Station TCR-405. Although limited to a measurement resolution of 1 mm, this device was able to verify the planarity of the vertical wall surface to which the target grid was mounted.

Along with the design of high-contract targets, uniform, diffuse lighting of the test object helps to maximize the precision with which the centroid of each tracked target can be identified in each image. Diffuse light sources help to minimize shadowing that can reduce the contrast between each target and the image background. Halogen work lights mounted around the perimeter of the workspace are an inexpensive, yet flexible method of accomplishing this. Unlike either florescent or conventional incandescent lights, halogen light sources provide a high-intensity, flicker-free illumination. To avoid overexposing the image, the halogen fixtures were connected to a Variac (variable voltage transformer), which functioned as a single dimmer control for the light array. Figure 3 shows a lighting scheme that includes halogen sources distributed above, below, and even behind the test article.

Although the videogrammetry software uses a referencing method that enables sub-pixel accuracy, there is still an inherent uncertainty that defines a baseline minimum for the measurement resolution in each direction. An

empirical method of determining these baselines for a particular experiment is to simply track the (apparent) motion of a stationary point. Tracking the apparent motion of the highest point in the coordinate grid shown in Figure 4 through all 1240 image epochs taken during the 12.1 Hz experiment, the Root Mean Square (RMS) of the position variation measured for this stationary point was 0.0248 mm, and the RMS values of the individual components of this "motion" were computed as 0.00792 mm (x-component); 0.01444 mm (y-component); and 0.01858 mm (z-component). Note that this measure of apparent motion of the physically fixed points as defined here is equivalent to standard deviation, and hence represents a 68.3% confidence level for all of the video-based position measurements reported herein. Confidence intervals for the acceleration measurements are frequency dependent, as they are computed directly from the positional tracking discussed previously. As harmonic, single frequency excitations were used in this set of experiments, 68.3% confidence intervals for the video-based acceleration data were determined for each component direction by simply multiplying the displacement confidence intervals by the square of the circular driving frequencies. The resulting acceleration confidence intervals are listed in Table I.

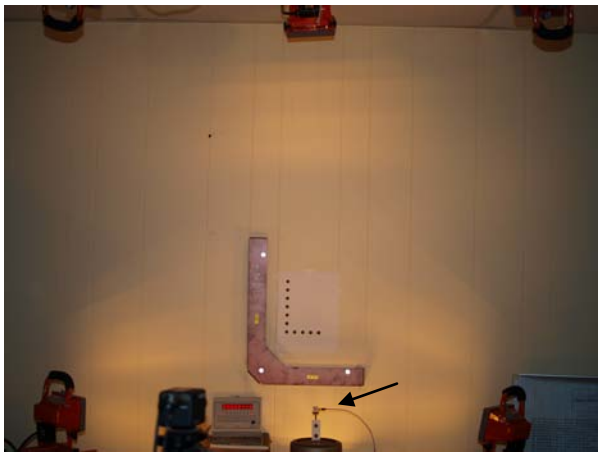

Fig. 3: Uniform, shadow-free illumination of a test object (accelerometer and shaft mounted on mechanical shaker, demarcated by arrow) was accomplished by using an array of eight (five visible) distributed halogen worklights, including one located directly behind the shaker. The upper set of lights was clamped directly to the ceiling tile grid.

Table I: Acceleration confidence limits at the excitation frequencies used in this series of tracking experiments.

	Acceleration Confidence Interval Components		
Component	**10.38 Hz [m/s^2]**	**12.1 Hz [m/s^2]**	**18.07 Hz [m/s^2]**
x	0.034	0.046	0.102
y	0.061	0.083	0.186
z	0.079	0.107	0.240

III. Computer Modeling and Correlation

III.A. Three-Dimensional Position Tracking

For each system studied, PhotoModeler6 was used to identify and track the three-dimensional location of each point demarcated by a high-contrast target. Videogrammetry projects performed within PhotoModeler are typically conducted in two phases: initial model reconstruction (using the first image from each camera, which are collectively referred to as the first *epoch*), followed by target tracking, using all remaining photosets (epochs). Once the user has identified the centroid of every point visible in each image contained in the first epoch (Figure 4A), PhotoModeler determines the three-dimensional location of each point using the known intrinsic camera characteristics and the principles of triangulation (Figure 4B). Absolute scale was ascertained using the known (measured) distances between the fixed points, and the model orientation was defined based on the relative positions of the fixed points. All epochs subsequent to the first were used for tracking; it was assumed that any points used to establish scale and orientation would remain stationary through the entire image sequence. In the example shown in Figure 4, the moving targets, located on the shaker-mounted oscillating shaft, were tracked (with sub-pixel accuracy) through the remaining frames. After all tracking was completed, PhotoModeler constructed a table for each epoch listing the points in the order they were marked, as well as the three-dimensional position of each.

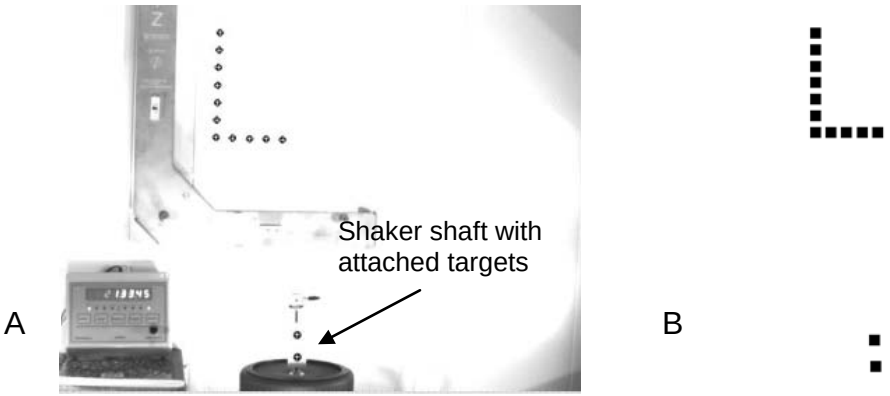

Fig. 4: (A) The centroid of each target shown in this Epoch 1 image has been marked with a plus (+) within PhotoModeler. (B) The static three-dimensional reconstruction of the point location was accomplished within PhotoModeler using all three images of Epoch 1.

III.B. Accelerometers

In order to provide a basis of comparison for the videogrammetry-based acceleration data, the experiments described herein utilized an accelerometer interfaced to an Iotech Wavebook516 16-bit Data Acquisition System through a WBK14 expansion module. The Piezotronics U339B01 triaxial ICP accelerometer has a resolution of 0.002g between 1 Hz and 2 kHz, and has sensitivities in the x, y and z directions of 90.8 mV/g, 89.1 mV/g, and 90.9 mV/g, respectively. Although the data acquisition board used has a maximum sampling rate of 1MHz, a 1 kHz per channel sampling rate was chosen.

III.C. Computing Acceleration from Position via Numerical Differentiation

In order to determine acceleration from the videogrametrically-measured position data, we chose the approach of differentiating the position data twice, using a simple numerical algorithm. While differentiation is an inherently noisy operation, this approach has been used successfully in the past to compute velocities from experimentally-determined position data. For instance, Alexander and Colbourne [12] differentiated experimentally-determined position data for several locations on a human limb segment, in order to obtain linear and angular velocities of the limb. While no examples reporting the use of videogrammetric position data to obtain acceleration information were found in the literature, there is no technical reason why this computation cannot be accomplished, as long as appropriate numerical processing schemes are used to mitigate the noise amplified by the successive differentiations.

IV. Experimental

The experiments performed consisted of attaching the triaxial accelerometer to a Vibration Research Corporation modal shaker, which was driven by a Wavetek FG3B signal generator and a Vibration Research Corporation VR565 driver. A threaded hole in the accelerometer enabled it to be screwed directly in to one of the threaded shafts provided with the shaker. The Wavetek signal generator has a frequency range of 0.2 Hz to 2 MHz; however, the operating frequency was chosen to be approximately 10% - 20% of the Nyquist frequency (100 Hz) limitation imposed by the cameras' sampling rate of 200 frames per second. A high-contrast, paper target was mounted to the shaker shaft using double-sided tape, directly under the accelerometer attachment point (Figure 4).

IV.A. Y-axis Alignment

The most basic experiment was designed so that the modal vibration was aligned with the y-axis of the coordinate system established within PhotoModeler. This was done to enable a simple comparison between the acceleration obtained using the twice-differentiated y-component of the videogrammetric position measurement, and that measured using the y-channel of the accelerometer. For this experiment, the cameras were arranged around the perimeter of the apparatus in the fashion previously described (Figure 1) to provide the three distinct views shown in Figure 5. That each camera is located in a different plane is most easily discerned by examining the orientation of the digital counter located on the left side of each image in Figure 5. For each of the two driving frequencies (12.1 Hz and 18.07 Hz) tested, 1242 epochs of simultaneously-acquired image sets (corresponding to 6.21 seconds) were captured by the videogrammetry system and stored on the computer hard drives. Concurrently, the Wavebook was used to collect three-channel data (x,y and z) from the accelerometer.

IV.B. Off-Axis Vibration Alignment

A slight modification of the first experiment tested the ability of the videogrammetry system to monitor three components of acceleration simultaneously. This was done by rotating the shaker about its x- and z-axes by approximately 30 degrees (Figure 6). The alignment of the accelerometer did not change with respect to the shaft of the shaker. As before, approximately 1242 epochs of image sets were captured by the videogrammetry system, while the Wavebook simultaneously recorded the accelerometer responses to the 10.38 Hz input.

Fig. 5: Once set of the experimental images (epoch) used to calculate acceleration of a sinusoidally-driven shaker. In this experiment, the oscillating shaft was aligned with the horizontal (y) axis of the pictured coordinate axes.

Fig. 6: Experimental images used to calculate off-axis acceleration of a sinusoidally-driven shaker. In this experiment, the shaker was rotated by 30 degrees with respect to both the x- and z-axes defined for the space. Both the lighting schemes and camera positions were slightly different than those chosen for the on-axis shaker experiment.

V. Results and Discussion

V.A. Acceleration at the Tip of a Sinusoidally-Driven Modal Shaker (Y-Axis Alignment)

The video sequences of the oscillating shaker shaft captured during this series of experiments were tracked using the videogrammetry software. Because of its alignment, the ideal shaft tracking should have contained only y-components of motion. The presence of any x- or z- components is therefore indicative of misalignment between the vibrating shaft and the wall-mounted coordinate axis. After subtracting out the constant x-, y- and z-offsets from each tracking run (determined by computing each mean displacement component relative to the specified origin of the coordinate axis), the first 0.5 seconds of the individual motion components measured from the two tests were plotted, and are shown in Figures 7 and 8, alongside their respective spectra obtained via Fourier analysis. In both cases, the z-components of the motion seem to be comprised primarily of random noise in the time domain, although their spectra indicate the presence of significant content at the driving frequency and harmonics superimposed on the full-spectrum noise band. Both the y- and the x-components are comprised primarily of the fundamental and harmonics, accompanied by relatively little noise. This indicates that the shaker shaft had a slight x-direction orientation. In both cases, the tracked motion in both the x- and z- directions are almost two orders of magnitude lower than the y-component of motion, indicating good (but not perfect) alignment of the reference axis with the vertical and horizontal directions. Alignment between the shaker and fixed coordinate system was accomplished through the use of the Total Station described in Section II.

As differentiation is an inherently noisy process, the approach chosen to numerically convert the tracked displacements to acceleration can significantly affect the quality of the results, which can then be evaluated via comparison to the accelerometer signal. Most numerical approaches for differentiation (as well as many for smoothing/filtering) operate sequentially point-by-point through a dataset, and modify each value in the set using a number of both prior and subsequent data points in the stream. A consequence of such an approach is that it cannot be used to calculate the accelerations at the endpoints of the dataset [14]. Some of these techniques can require the removal of up to 15 points at each end of the sequence. While this may not be important for evaluating repeating motions such as that of the oscillating shaker presented here, the loss of up to 30 epochs of video (15 on each end) to smoothing and differentiation can represent a significant part of the tracking data for brief, transient motion events such as that initiated by an impact force. In addition, when selecting one of these approaches, care must be taken to ensure that the numerical smoothing removes noise while preserving the true features of the waveform. These issues should be considered when choosing the combination of algorithms used to calculate acceleration from the videogrammetrically-tracked position.

V.A.i. Determination of Acceleration via Numerical Differentiation Alone

Seven-point numerical differentiation alone (without filtering or smoothing) was used to initially calculate the three Cartesian acceleration components from the tracked target position values extracted from the videogrammetry data [13]:

$$f''_i = \frac{2f_{i-3} - 27f_{i-2} + 270f_{i-1} - 490f_i + 270f_{i+1} - 27f_{i+2} + 2f_{i+3}}{180\Delta t^2} \quad (1)$$

where f''_i is the numerically-computed second derivative at point i, f_{i-3} through f_{i+3} are the ordinate locations for consecutive points of tracked position data, and Δt is the fixed change in the abscissa between two adjacent points (determined here by the respective sampling rates of the data acquisition techniques). The differentiation algorithm was implemented using a simple engineering spreadsheet. The calculated components of acceleration, along with their spectral content, are shown in Figures 9 and 10. At both frequencies, the spectral content of y-component of acceleration consists mainly of the driving frequency, although some increase in high frequency noise content is apparent. However, the off-axis x- and z- motion (due to misalignment of the axis), when differentiated, yield the driving frequency, prominent harmonics, as well as a great deal of high-frequency noise

content. In the time-domain, it is not clear that any meaningful acceleration information can be discerned from the x- or z- trackings. It is also clear that the noise superimposed on the position data (Figures 7 and 8) is amplified by the double-differentiation process, an effect that is more pronounced at higher frequencies (Figures 9 and 10).

V.A.ii. Determination of Acceleration via Numerical Differentiation of Smoothed Tracking Measurements

Prior work done by Kienle et al. [15] suggests that numerical filtering could be used to improve the results of obtained when videogrammetry-based displacement data are twice differentiated to obtain accelerations. Filtering prior (rather than subsequent) to differentiation was chosen because high-frequency noise components caused by inherent measurement uncertainty tend to be significantly magnified by the differentiation process. An appropriate filter must be chosen so that the fundamental deflection path recorded by the measurement is not significantly attenuated by the filtering process. Furthermore, in order to accommodate excitations that have a broader spectral content than the pure sinusoids utilized here (chosen for ease of implementation and repeatability in this proof-of-concept study), low-pass filters were deemed to be inappropriate for this application. In contrast, windowing approaches incorporating the calculation of moving averages are considered to be optimal for the reduction of superimposed noise while maintaining even the underlying high-frequency components of the measured motion [16]. However, filters incorporating a simple moving-window-averaging approach are only appropriate for monotonically increasing or decreasing functions whose second derivatives are expected to be zero. Hence, using simple averaging filters on data that contain local peaks always causes the magnitude of those peaks to decrease. [17] However, there are other similar approaches that (at least partially) mitigate this peak reduction. In such an extension of the simple averaging approach, Savitzky and Golay were among the first to propose that the effects of random noise on experimental data could be minimized

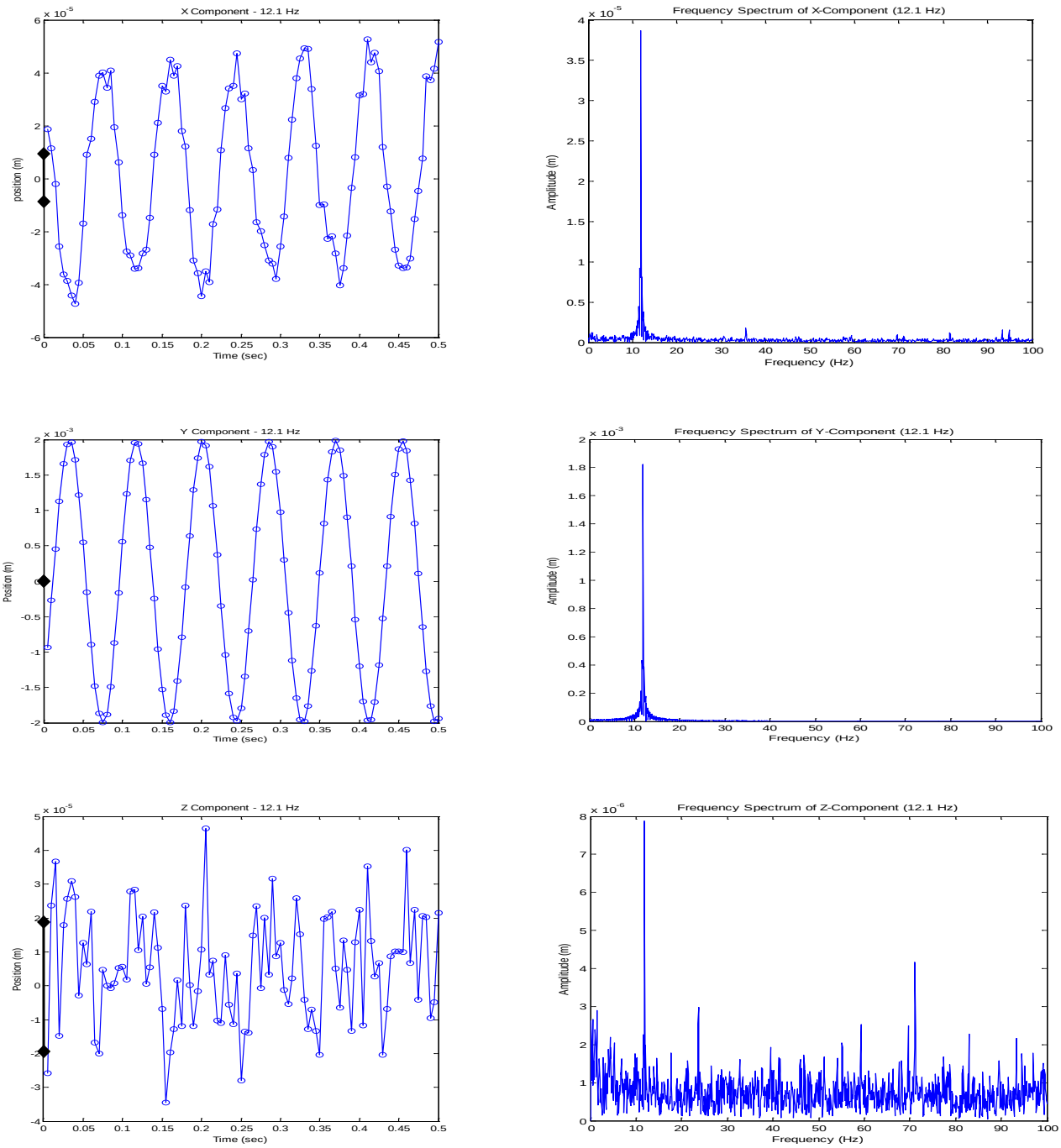

Fig. 7: x-, y- and z-component videogrammetric-based tracking results for a 12.1 Hz y-axis harmonic motion. 68.3% confidence levels (of +/-7.92 μm, +/-14.4 μm, and +/-18.6 μm respectively for the x- y- and z-directions) are shown to scale on their respective ordinates. The tracked motion in the x- and z- directions (non-driven) are almost two orders of magnitude lower than the y-component of motion, indicating good alignment of the reference axis with the vertical. However, the 12.1-Hz component apparent in the top plot does indicate a small component of shaft displacement along the defined x-axis, indicating a slight misalignment between the axis of the shaker and the specified coordinate system. Fourier analysis shows that the spectral content of the z-component also contains the fundamental, even though it is not apparent through simple inspection of the time-domain signal. The z-component of the response also includes a great deal of noise.

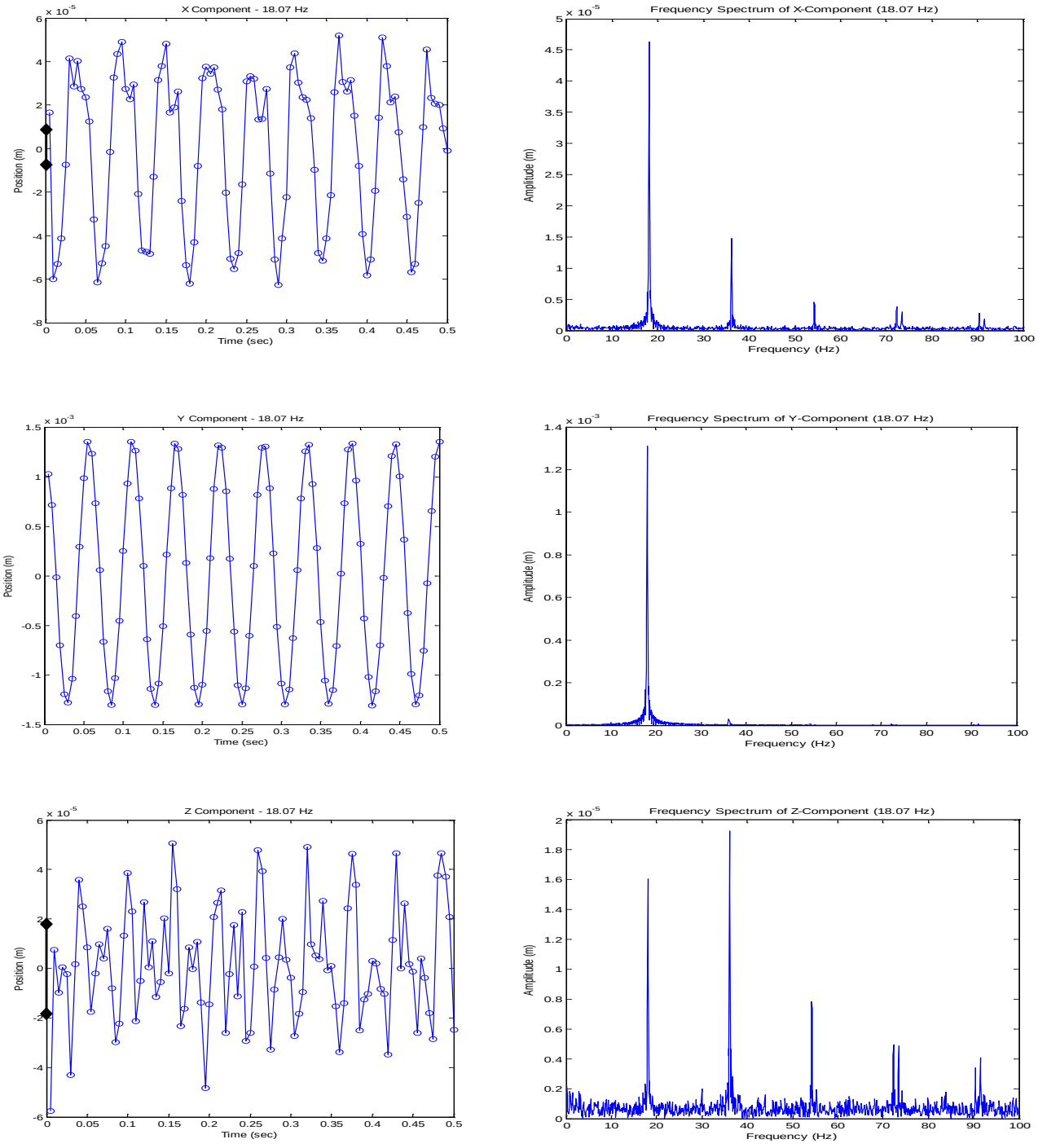

Fig. 8: x-, y- and z-component videogrammetric-based tracking results for an 18.07 Hz y-axis harmonic motion. 68.3% confidence levels (of +/-7.92 μm, +/-14.4 μm, and +/-18.6 μm respectively for the x- y- and z-directions) are shown to scale on their respective ordinates. The tracked motion in the x- and z- directions (non-driven) are almost two orders of magnitude lower than the y-component of motion, indicating good alignment of the reference axis with the vertical. However, the 18.07-Hz component apparent in the top plot does indicate a small component of shaft displacement along the defined x-axis, indicating a slight misalignment between the axis of the shaker and the specified coordinate system. Spectral analysis indicates that both off-axis responses have induced harmonics at integer multiples of the driving frequency. The z-component of the response also includes a great deal of noise.

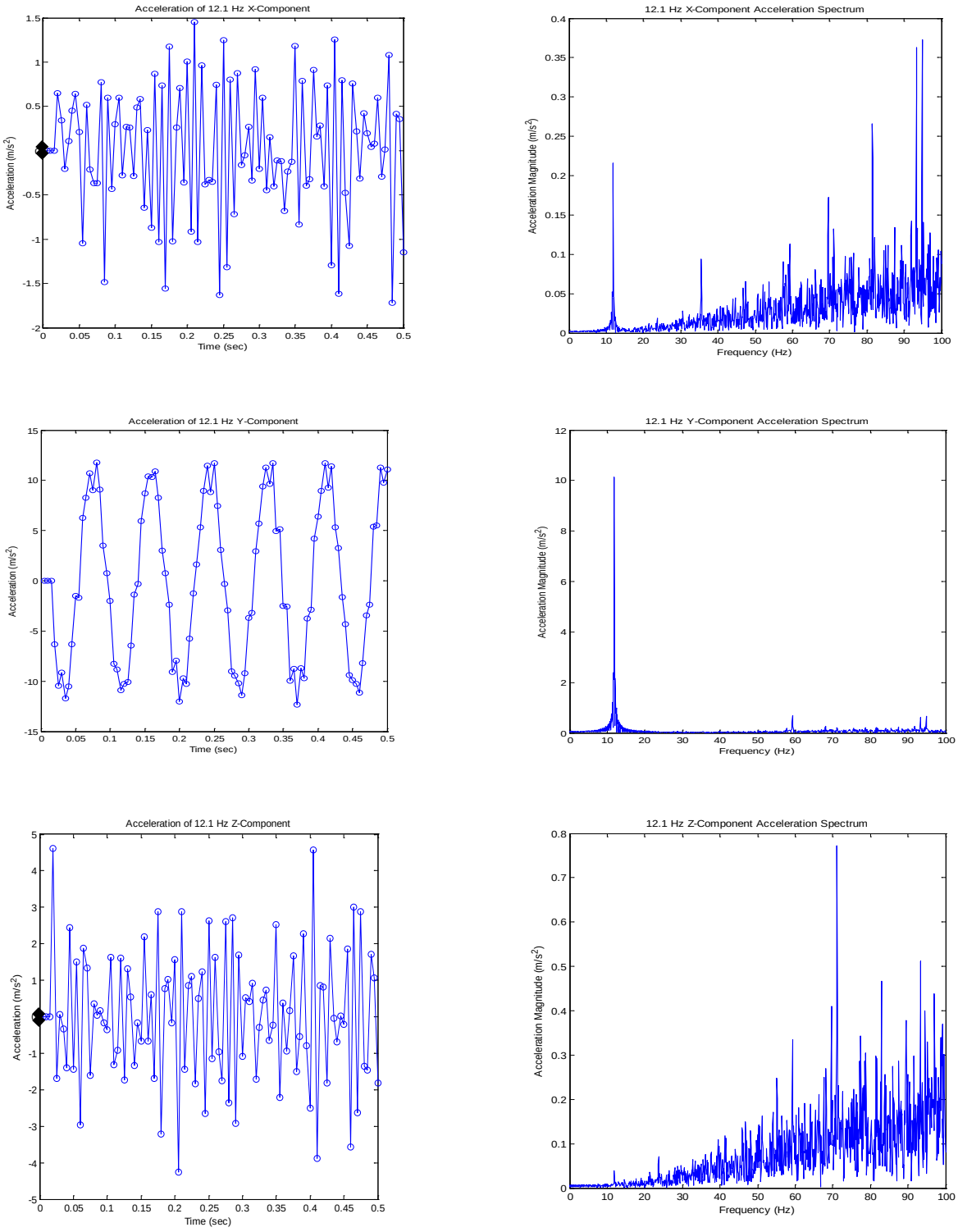

Fig. 9: Components of acceleration of 12.1 Hz oscillation obtained by 7-point numerical differentiation algorithm. 68.3% confidence levels (of +/-0.046 m/s^2, +/-0.083 m/s^2, and +/-0.107 m/s^2 respectively for the x- y- and z-directions) are shown to scale on their respective ordinates. While the x- and y- acceleration spectra reflect the 12.1 Hz driving frequency (as well as higher frequency noise), the z-component acceleration spectrum consists primarily of high-frequency noise.

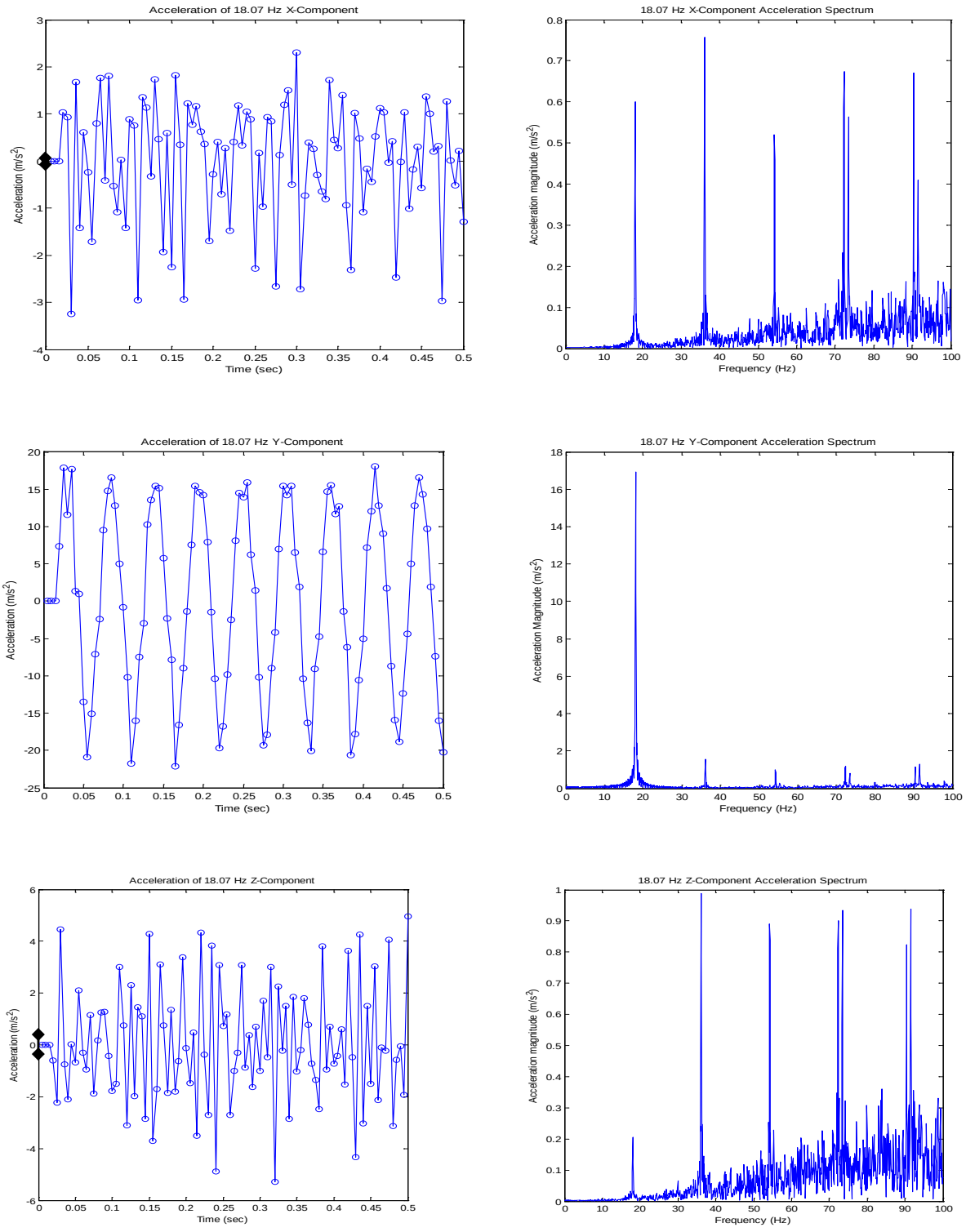

Fig. 10: Components of acceleration of 18.07 Hz oscillation obtained by 7-point numerical differentiation algorithm. 68.3% confidence levels (of +/-0.102 m/s^2, +/-0.186 m/s^2, and +/-0.240 m/s^2 respectively for the x- y- and z- directions) are shown to scale on their respective ordinates. The y-component spectrum consists primarily of the driving frequency (though some induced harmonic content is apparent); the x- and z- components contain both harmonics and high-frequency noise components that swamp the 18.07 Hz fundamental.

through a least-squares approach that smoothed the data while substantially retaining the precise features of the curve – including the peaks [18,19]. Although the videogrammetric-based tracking data shown in Figures 7 and 8 for the y-direction look smooth, even that motion component contains superimposed noise content similar to that discussed by Savitzky and Golay, which arises, here, from the inherent uncertainty in the measurement. This uncertainty was discussed previously, and was clearly demonstrated by tracking the apparent motion of a stationary point. Comparing the 68.3% displacement confidence values for each motion component obtained previously to the RMS values of the measured motions shown in Figure 7 (which are respectively 0.0304 mm, 1.414 mm and 0.01644 mm for x-, y- and z- components at the 12.1 Hz driving frequency), the noise-floor for the x- y- and z-components respectively represented 26%, 1% and 113% of the tracked motion components. Based on this approach, the z-component of (apparent) motion depicted in Figures 7 and 8 can be attributed primarily to random tracking error. In contrast, the noise components superimposed on the harmonic x- and y- motions (that stem from the same mechanism of random tracking error) may be small enough to be removed by one of the proposed smoothing functions. The values for the minimum tracking resolution (noise floor) in each direction are also relevant because they provide perspective on the relative size of the modifications to the displacement component values induced by each of the applied smoothing functions.

In choosing an appropriate Savitzky-Golay filter for a particular application, Persson and Strang state that the window length (n) must correspond to the length of the shortest feature of interest (to be preserved) in the input signal [20]. For instance, for a Gaussian input with superimposed white noise, they state that effective filter length corresponds to the width of the Gaussian at its half-maximum point. Here, the inputs are sinusoidal with approximately 7-8 samples per half-cycle; hence the appropriate filter length is n = 7, as using a longer filter will more significantly reduce the amplitude of the waveform being filtered. In contrast, the only effect of using a filter whose length is too short will be its reduced effectiveness in eliminating the high-frequency noise components. A seven-point Savitzky-Golay filter was therefore applied to the x- and y- components of the tracked target motion plotted in Figures 7 and 8. The equation for this filter is provided below:

$$f_{si} = \frac{-2f_{i-3} + 3f_{i-2} + 6f_{i-1} + 7f_i + 6f_{i+1} + 3f_{i+2} - 2f_{i+3}}{21} \quad (2)$$

where f_{si} is the value of the smoothed function at point i, and f_{i-3} through f_{i+3} are the ordinate locations for consecutive points of tracked position data used to generate each least-squares smoothing function that together comprise the filter. The smoothed x, y and z components of the 12.1 Hz and 18.07 Hz displacement data are shown, together with their respective Fourier spectra, in Figures 11 and 12. The accelerations obtained from the smoothed displacement functions are shown, together with their Fourier spectra, in Figures 13 and 14.

At both frequencies, comparison of Figures 7 and 8 with Figures 11 and 12 indicates that the y-component of the target displacement appears to be virtually unaffected by the numerical filtering process, at least in the time-domain. Careful comparison of the y-component displacement spectrum in Figure 8 versus Figure 12 indicates that the Savitzky-Golay does successfully attenuate high-frequency noise components without suppressing the underlying measured motion. In contrast, the measured x-components of the tracked displacement at 12.1 Hz and 18.07 Hz are clearly "cleaned up" by the filtering process. Comparison of the spectra shows that high frequency components, especially above 30 Hz, have been significantly reduced by the filtration. Finally, although the high-frequency z-components of tracked motion also decrease after Savitzky-Golay filtering, the filtered tracking is still not visibly identifiable as a pure sinusoid in the time domain. As discussed previously, this is because the RMS value of the tracking error in the z-direction was similar in magnitude to the RMS value of the tracked Z-motion component. Hence there was little meaningful underlying z-component that filtration could help to reveal.

Numerical calculation of acceleration using the unfiltered (Figures 9 and 10) versus the filtered (Figures 13 and 14) data shows how significant prefiltering the displacement data is in reducing the presence of high-frequency noise in the accelerations computed using Equation 1. High-frequency content visible on the y-component in both

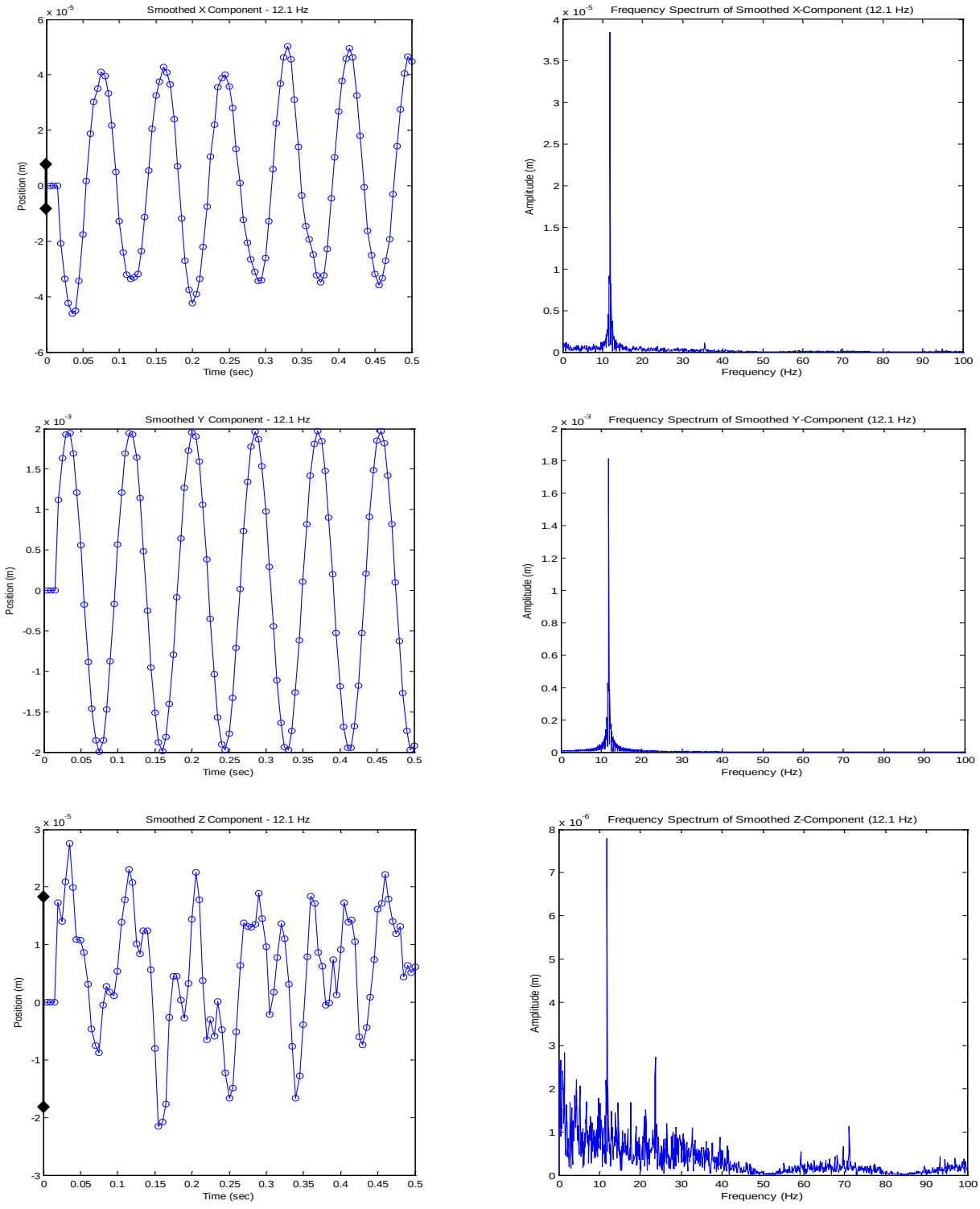

Fig. 11: Position data smoothed through Savitzky-Golay filter for 12.1 Hz oscillation (compare with unfiltered data in Figure 7). 68.3% confidence levels (of +/-7.92 μm, +/-14.4 μm, and +/-18.6 μm respectively for the x- y- and z- directions) are shown to scale on their respective ordinates.

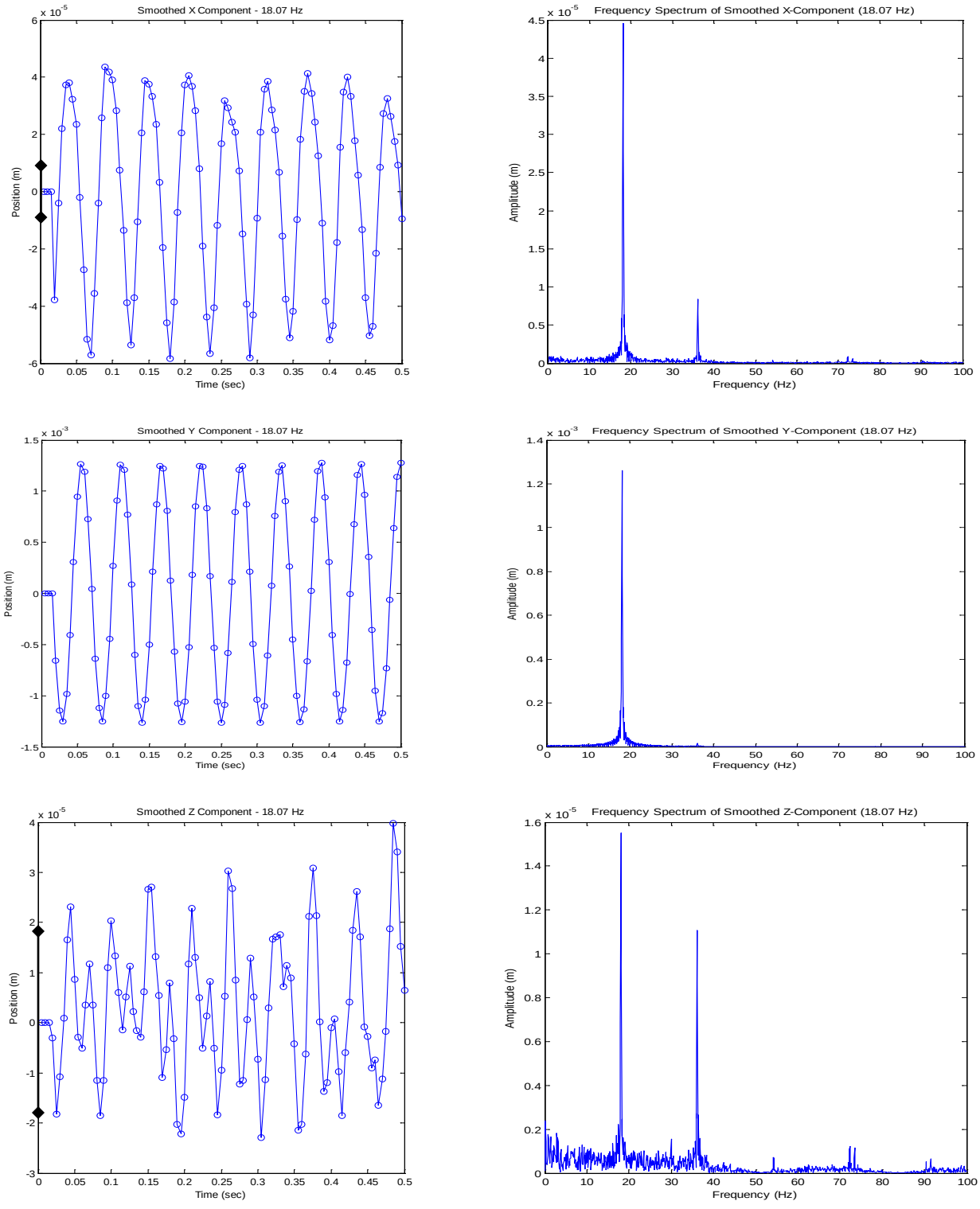

Fig. 12: Position data smoothed through Savitzky-Golay filter for 18.07 Hz oscillation (compare with unfiltered data in Figure 8). 68.3% confidence levels (of +/-7.92 μm, +/-14.4 μm, and +/-18.6 μm respectively for the x- y- and z- directions) are shown to scale on their respective ordinates.

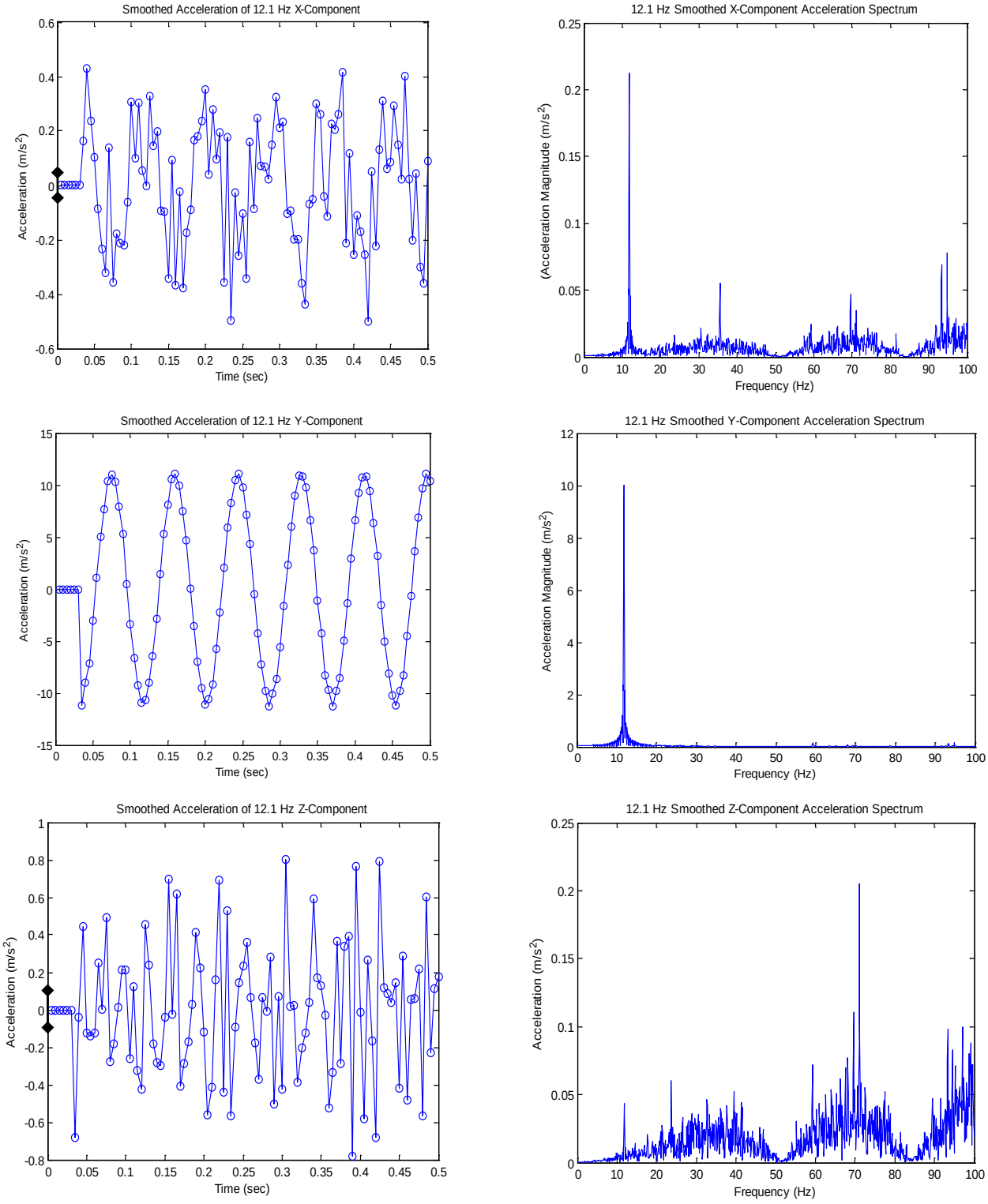

Fig. 13: Acceleration data obtained by twice-differentiating smoothed position data for 12.1 Hz oscillation (from Figure 11); compare with acceleration profile (Figure 9) obtained from unfiltered position data. 68.3% confidence levels (of +/-0.046 m/s^2, +/-0.083 m/s^2, and +/-0.107 m/s^2 respectively for the x- y- and z-directions) are shown to scale on their respective ordinates.

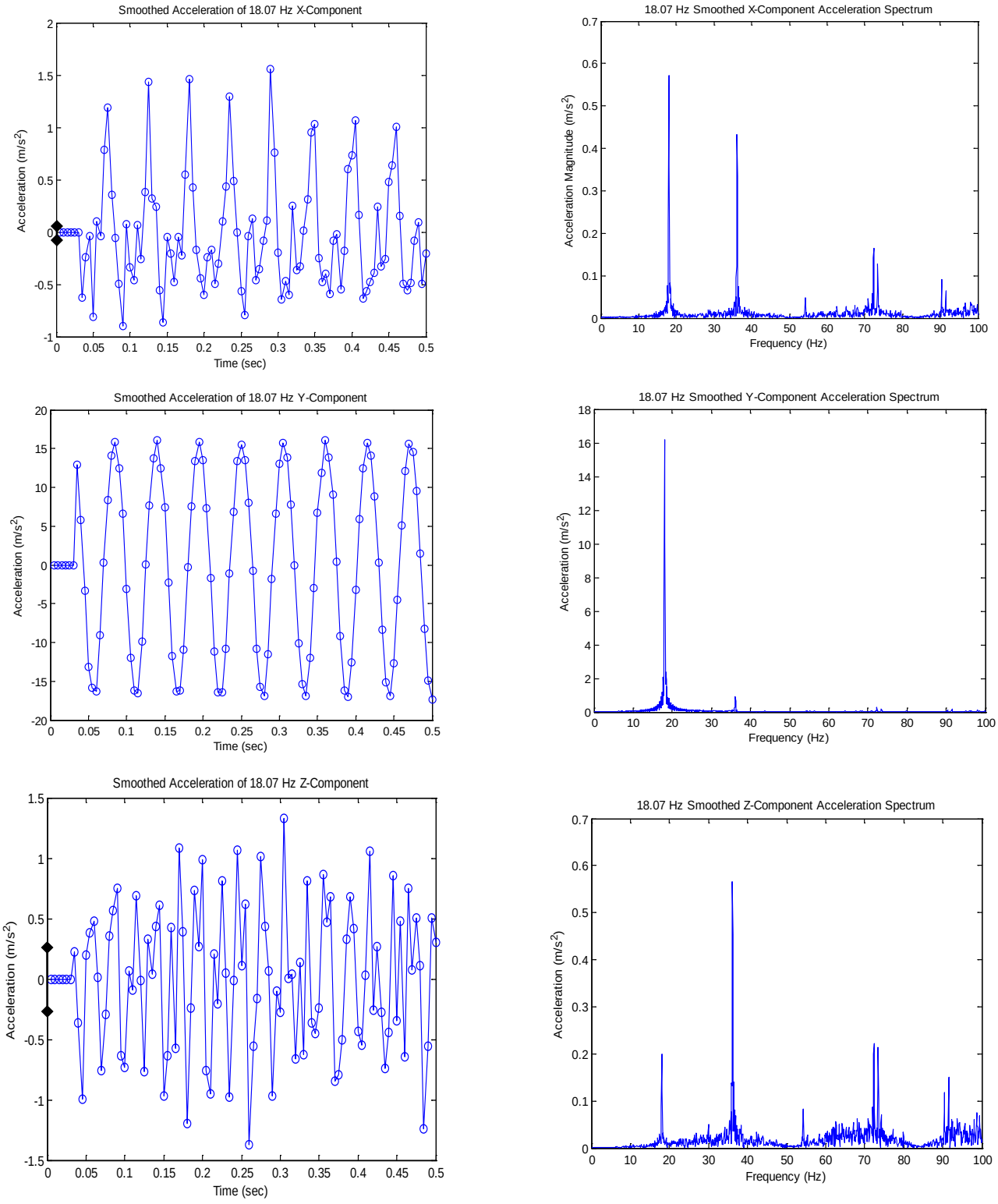

Fig. 14: Acceleration data obtained by twice-differentiating smoothed position data for 18.07 Hz oscillation (from Figure 12); compare with acceleration profile (Figure 10) obtained from unfiltered position data. 68.3% confidence levels (of +/-0.102 m/s^2, +/-0.186 m/s^2, and +/-0.240 m/s^2 respectively for the x- y- and z-directions) are shown to scale on their respective ordinates.

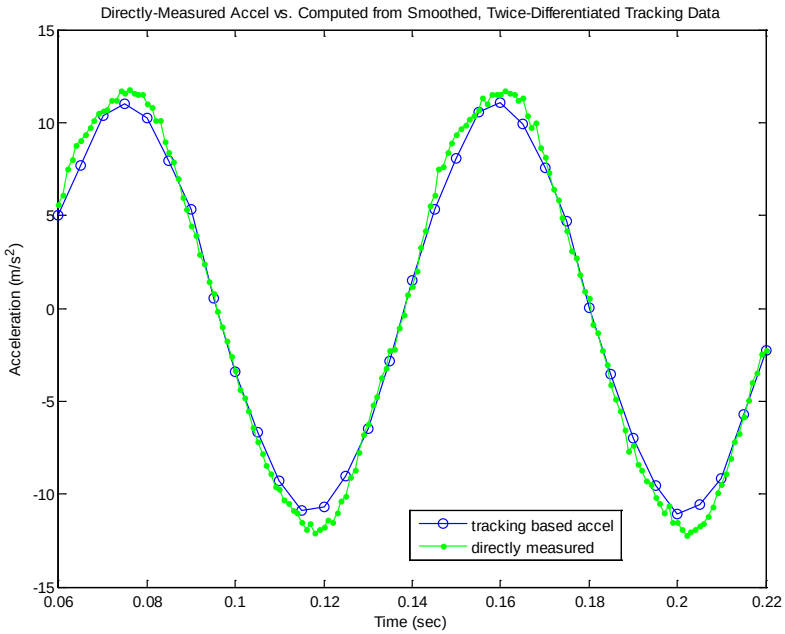

Fig. 15: Directly measured acceleration versus that computed using smoothed, twice-differentiated tracking data (for 12.1 Hz oscillation). The two acceleration measurements track well with each other, except at the vertices where the shaft is changing direction. The 68.3% confidence intervals for neither the video-based nor the accelerometer measurement are resolvable at this scale.

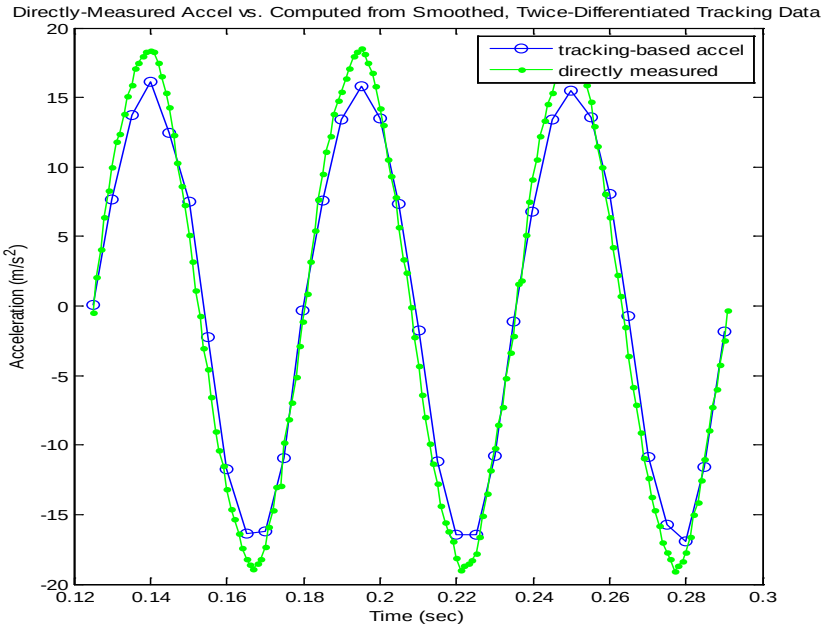

Fig. 16: Directly measured acceleration versus that computed using smoothed, twice-differentiated tracking data (for 18.07 Hz oscillation). The two acceleration measurements track well with each other, except at the vertices where the shaft is changing direction. The 68.3% confidence intervals for neither the video-based nor the accelerometer measurement are resolvable at this scale.

the time- and frequency- domains in Figures 9 and 10 is obviously reduced in Figures 13 and 14. For the x- and z- components, the primary effect of the filtering on the computed accelerations is visible in their respective frequency spectra.

Because the x-component of acceleration was a factor of 20 less than the y-component calculated using the smoothed tracking data (and hence contributed little to the total acceleration magnitude), the acceleration measured at the tip of the shaker shaft using the accelerometer was compared directly to that obtained by applying Equation 1 to the smoothed y-tracking data. These results are shown in Figures 15 and 16. It is apparent that there is good correlation between the video-tracking-based and directly-measured accelerations, although the former seems to underestimate the latter near the local displacement extrema, where the shaft reversed direction.

V.B. Acceleration at the Tip of a Sinusoidally-Driven Modal Shaker (Off-Axis Vibration Alignment)

As was the case for the primarily y-aligned shaft oscillation, the constant x-, y- and z-offsets from the off-axis tracking run (determined by computing each mean displacement component) were subtracted from each component of the video-based position data. Because each cycle of the waveform has a larger number of samples per period (due to the lower, 10.38 Hz excitation frequency) each recorded component of motion was smoothed using the 11-point Savitzky-Golay filtering algorithm [18,19]. The first two cycles of the individual motion components were then plotted (Figure 17). Acceleration components were computed using the 7-point central difference algorithm (Equation 1), and are shown in Figure 18. These acceleration components deviated from the ideal sinusoid, more than the acceleration component shown in Figure 15 (for the y-axis-aligned oscillation), especially at the extrema. However, the recognizable sinusoidal form of the accelerations shown in Figure 18 is a vast improvement over accelerations computed directly from the x-, y- and z- components of the displacement using Equation 1 alone (Figure 19).

In order to compare the videogrammetry-based acceleration measurements with that measured directly by the accelerometer, the components of the video-based accelerations, shown in Figure 17, were used to compute an acceleration magnitude, shown in Figure 20. These points are superimposed on to the shaft-acceleration directly

measured by the accelerometer. Except for near the peak acceleration values, the videogrammetry-based acceleration magnitudes coincided with the measured on-axis values.

V.C. Acceleration Magnitude

The experiments described in the previous sections demonstrate that the video-based techniques are capable of accurately obtaining acceleration values of between 1-g and 2-g when the noise component is pre-filtered from the tracked displacements prior to differentiation. Additional measurements will need to be performed to determine the upper measurement limit for this approach using this particular (or any similar) combination of equipment and processing algorithms. This would be especially useful for evaluating whether impact-induced motions, which can exceed 10g, can be resolved via videogrammetry-based acceleration measurement techniques. Furthermore, a frequency-response calibration curve similar to that provided with accelerometers could be developed to enable the lower and upper bounds for any equipment set to be determined. This could best be done by repeating the on-axis experiments described in Section V.A. using a number of different excitation frequencies above 18.07 Hz.

V.D. Single-Point versus Multiple Measurement Locations

As alluded to previously, one major advantage of videogrammetry-based accelerometer measurements is the ability to compute in- and out-of-plane acceleration components at any location on a moving target by simply installing markers at all locations of interest. While data for only one marker on the moving shaft were presented in this paper, two markers were included on the setups shown in Figures 3-6, and either of them could have been used to obtain the same results, as the shaft assembly was moving in essentially a rigid-body mode. The inclusion of multiple markers is most important for flexible structures that do not move in a uniform fashion, such as the etched film whose surface motion was evaluated using videogrammetry by Leifer et al [9].

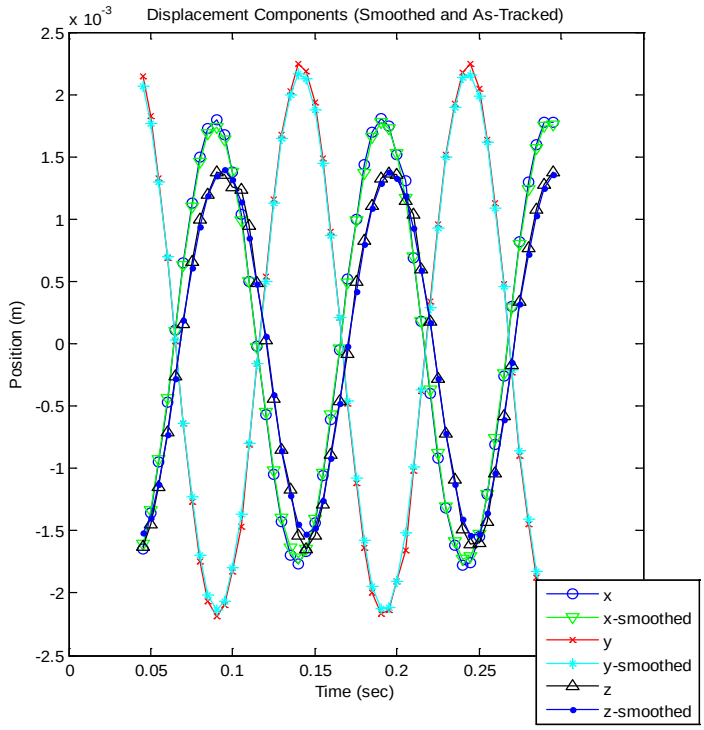

Fig. 17: Components of off-axis shaker oscillation showing both unsmoothed (as-tracked) and smoothed displacement functions. The 68.3% confidence intervals are not resolvable at this scale.

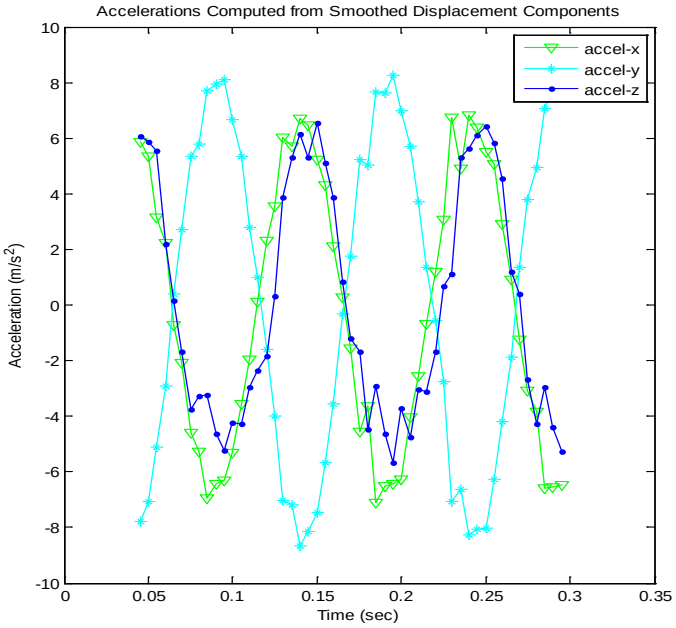

Fig. 18: The accelerations components of the off-axis shaker oscillation computed from the smoothed displacement components showed some noise at each cycle extreme, but otherwise possessed the expected phase-shifted sinusoidal shape. The 68.3% confidence intervals are not resolvable at this scale.

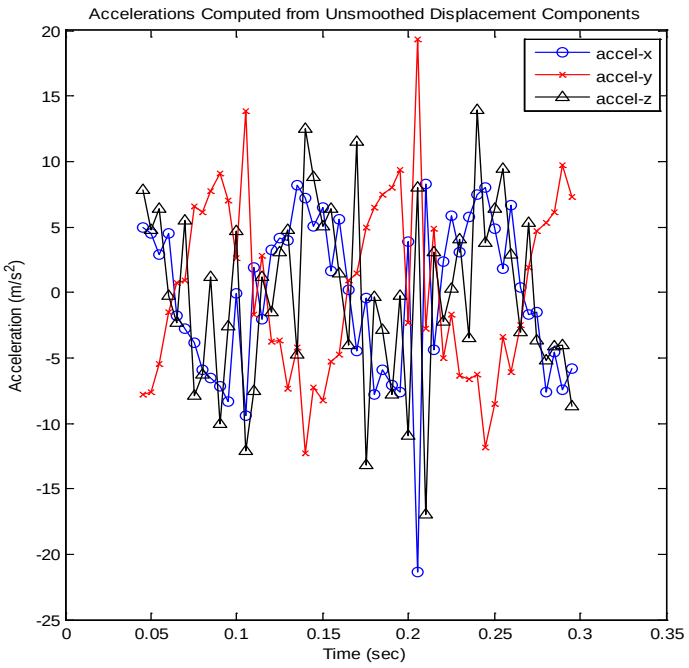

Fig. 19: The acceleration components of the off-axis shaker oscillation computed from the unsmoothed displacement components showed significant higher-order content, and were not readily identifiable as twice-differentiated sinusoids. The 68.3% confidence intervals are not resolvable at this scale.

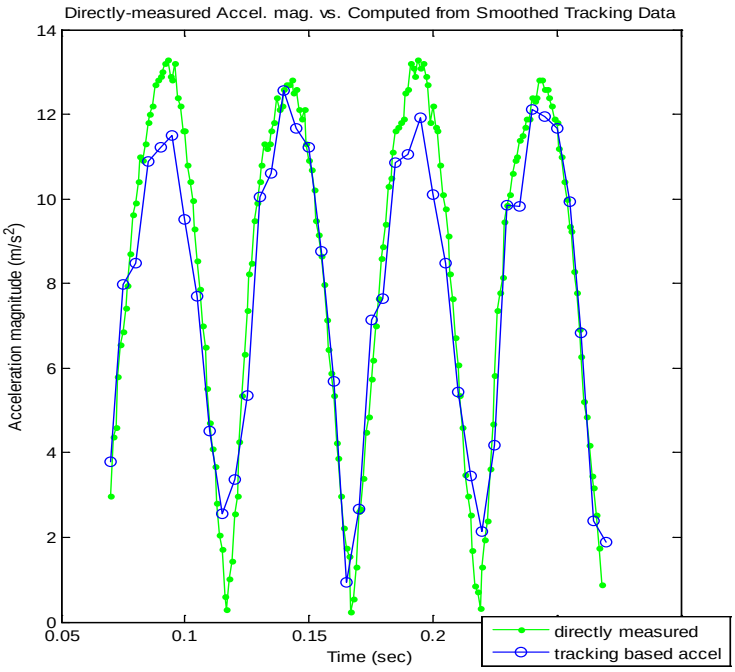

Fig. 20: Comparison of acceleration magnitudes: Directly measured using accelerometer, and acceleration magnitude calculated by twice-differentiating smoothed displacement components obtained through video tracking. The 68.3% confidence intervals for neither the video-based nor the accelerometer measurement are resolvable at this scale.

VII. Conclusion and Recommendations for Future Work

This results obtained from this set of preliminary experiments clearly show the potential of videogrammetry-based acceleration measurements, based on filtered, twice-differentiated position data. There are many different avenues for continuation of this research, some of which were discussed in the previous section. These include the following:

- Thorough investigation of additional filtering approaches for the displacement data, which could potentially reduce the noise (and increase the correlation) of the videogrammetry-based acceleration measurements.
- Investigation of the degradation in correlation between videogrammetry- and accelerometer-based measurements as the frequency content of the test-subject motion increases towards the 100Hz Nyquist frequency limit imposed by the camera frame-rate.
- Further characterization of in-plane acceleration components using videogrammetry-based measurements. Videogrammetry has a potential advantage over multi-axis accelerometers for measurement of in-plane acceleration components, because in a videogrammetry-based measurement, all components are evaluated relative to a set of invariant coordinate axes defined for the project. While multi-axis accelerometers can measure individual acceleration components, they can rotate with the test object. This can substantially complicate data interpretation.
- Comparison of forces calculated using videogrammetry-based acceleration measurements with force measured simultaneously using conventional sensors.
- Implementation of this approach using inherent (markerless) targeting techniques. This would eliminate the need for placing targets on the surface of the moving test articles.

Acknowledgements

The authors are grateful for support through Trinity University's Howard Hughes Medical Institute (HHMI) program, as well as the Trinity University Office of Academic Affairs. Additional support was provided through the William Liston Zander Faculty Fellowship for Summer Research.

References

1. Denoyer KK, Flint EM, Main JA, Lindler J (2003) Actively controlled thin-shell space optics. Proceedings of SPIE - The International Society for Optical Engineering 5054: 263-274.

2. Dharamsi, UK, Evanchik, DM, and Blandino, JR (2002) Comparing photogrammetry with a conventional displacement measurement technique on a square kapton membrane. Paper 2002-1258, Proceedings of the 3rd AIAA Gossamer Structures Forum, Denver, CO.

3. Jenkins, CH, Haugen, F, and Spicher, WH (1998) Experimental measurement of wrinkling in membranes undergoing planar deformation. Experimental Mechanics, 38(2): 147-152.

4. Schmidt, T, Tyson, J, and Galanulis, K (2003) Dynamic strain measurement using advanced 3D photogrammetry. Proceedings of IMAC XXIII: The 21st International Modal Analysis Conference, Orlando, FL.

5. Black JT, Pappa RS (2003) Videogrammetry using projected circular targets: proof-of-concept test. NASA/TM-2003-212148

6. Kay IW, Zobel EC (1973) Simplified three-dimensional photogrammetric analysis of moving bodies. Paper 730278, Society of Automotive Engineers International Automotive Engineering Congress, Detroit, MI

7. Miller NR, Shapiro R, McLaughlin TM (1980) A technique for obtaining spatial kinematic parameters of segments of biomechanical systems from cinematographic data. Journal of Biomechanics 13:535-547

8. Mesqui F, Niederer, P, Schlumpf M, Lehareinger Y, Walton, J (1984) Semi-automatic reconstruction of the spatial trajectory of an impacted pedestrian surrogate using high-speed cinephotogrammetry and digital image analysis. Journal of Biomechanical Engineering 106:357-359

9. Leifer J, Black JT, Smith SW, Ma N., Lumpp JK (2007) Measurement of in-plane motion of thin-film structures using videogrammetry. AIAA Journal of Spacecraft and Rocket 44:1317-1325

10. Mikhail, EM, Bethel, JS, McGlone JC (2001) Introduction to modern photogrammetry. John Wiley and Sons, New York

11. Anonymous (2006) PhotoModeler version 6 users' manual. Eos Systems, Vancouver, BC.

12. Alexander MJL, Colbourne J (1980) A method of determination of the angular velocity vector of a limb segment. Journal of Biomechanics 13:1089 – 1093

13. Griffiths DV, Smith IM (2006) Numerical methods for engineers, CRC Press, 221

14. Palm, WJ III (2005) Introduction to matlab 7 for engineers. McGraw-Hill, New York

15. Kienle SC, Sims AM, Leifer J (2008) Full-field acceleration measurement using videogrammetry. Proceedings of IMAC XXVI: The 26th International Modal Analysis Conference, Orlando, FL

16. Smith, SW (2002) Digital signal processing: A practical guide for engineers and scientists. Newnes. Also available at www.dspguide.com (accessed 22 FEB 2010).

17. Press, WH, Teukolsky, SA, Vetterling, WT, Flannery, BP (1992) Numerical recipes in FORTRAN: The art of scientific computing, Second Edition. Cambridge University Press

18. Savitzky A, Golay MJE (1964) Smoothing and differentiation of data by simplified least squares procedures. Analytical Chemistry 36:1627 - 1639

19. Steiner J, Termonia Y, Deltour J (1972) Comments on smoothing and differentiation of data by simplified least square procedure. Analytical Chemistry 44: 1906 – 1909

20. Persson, P-O, Strang, G (2003) Smoothing by Savitzky-Golay and Legendre filters. The IMA Volumes in Mathematics and its Applications, 301 – 315.